B.M. Verbist
R.M.S. Joemai
W.M. Teeuwisse
W.J.H. Veldkamp
J. Geleijns
J.H.M. Frijns

Evaluation of 4 Multisection CT Systems in Postoperative Imaging of a Cochlear Implant: A Human Cadaver and Phantom Study

BACKGROUND AND PURPOSE: Postoperative imaging of cochlear implants (CIs) needs to provide detailed information on localization of the electrode array. We evaluated visualization of a HiFocus1J array and accuracy of measurements of electrode positions for acquisitions with 64-section CT scanners of 4 major CT systems (Toshiba Aquilion-64, Philips Brilliance-64, GE LightSpeed-64, and Siemens Sensation-64).

MATERIALS AND METHODS: An implanted human cadaver temporal bone, a polymethylmethacrylate (PMMA) phantom containing a CI, and a point spread function (PSF) phantom were scanned. In the human cadaver temporal bone, the visibility of cochlear structures and electrode array were assessed by using a visual analog scale (VAS). Statistical analysis was performed with a paired 2-tailed Student t test with significant level set to .008 after Bonferroni correction. Distinction of individual electrode contacts was quantitatively evaluated. Quantitative assessment of electrode contact positions was achieved with the PMMA phantom by measurement of the displacement. In addition, PSF was measured to evaluate spatial resolution performance of the CT scanners.

RESULTS: VAS scores were significantly lower for Brilliance-64 and LightSpeed-64 compared with Aquilion-64 and Sensation-64. Displacement of electrode contacts ranged from 0.05 to 0.14 mm on Aquilion-64, 0.07 to 0.16 mm on Brilliance-64, 0.07 to 0.61 mm on LightSpeed-64, and 0.03 to 0.13 mm on Sensation-64. PSF measurements show an in-plane and longitudinal resolution varying from 0.48 to 0.68 mm and 0.70 to 0.98 mm, respectively, over the 4 scanners.

CONCLUSION: According to PSF results, electrode contacts of the studied CI can be visualized separately on all of the studied scanners unless curvature causes intercontact spacing narrowing. Assessment of visibility of CI and electrode contact positions, however, varies between scanners.

Multisection CT (MSCT) has proven its efficacy in the postoperative imaging of cochlear implant (CI) patients.[1,2] Like conventional x-ray, CT confirms the intracochlear position of the implant. It has also been shown that malpositioning and kinking can be detected by CT imaging.[1,3-5] In addition, MSCT provides important information on other clinical or research-based issues. By visualizing not only the individual electrode contacts but also the cochlear morphology and fine anatomic structures, valuable information is gained. The positioning of an electrode array, as well as the individual electrode contact-to-modiolus distance, can be assessed. This yields objective measurements facilitating the evaluation of differences in outcome (speech perception) after implantation of different types of electrode arrays.[6,7] New electrode designs, such as the split electrode, can be thoroughly examined.[8] The number of functional electrode contacts and an antegrade or retrograde course of the second array can be determined. Recently, the optimal size and spacing of electrode contacts for a new type of split array were determined with the help of such CT imaging (unpublished data). In addition, in cases of congenital cochleovestibular malformation, CT enables assessment of the surgical result with regard to the number of functional electrode contacts and rotation of the array. In this way, postoperative imaging by MSCT contributes to improvements of implant fitting, development of electrode designs, and assessment of surgical techniques.

Still, reservations toward the application of CT in these patients are widespread.[9-12] Concerns with regard to suboptimal image quality because of metallic artifacts exist, and it is not clear whether recent models of MSCT scanners and applied acquisition protocols produce adequate image quality for reliable assessment of CI placement.

In this study, the visualization of a HiFocus1J electrode array (Advanced Bionics, Sylmar, Calif) and the accuracy of measurements of electrode positions for acquisitions with 64-section CT scanners of 4 major CT systems (Aquilion-64 [Toshiba Medical Systems, Otawara, Japan], Brilliance-64 [Philips Medical Systems, Best, the Netherlands], LightSpeed-64 [GE Healthcare, Milwaukee, Wis], and Sensation-64 [Siemens Medical Solutions, Malvern, Pa]) were evaluated in a human cadaver temporal bone and in a polymethylmethacrylate (PMMA) phantom.

Materials and Methods

MSCT scans were performed on an implanted human cadaver temporal bone to evaluate the appearance of clinical images. To analyze the performance and resolution of 4 different 64-section CT scanners, point spread function (PSF) was measured for each CT scanner, and images of a CI embedded in a polymethylmethacrylate (PMMA) phantom of the basal turn of the cochlea were acquired.

Data Acquisition and Image Reconstruction

Scans were performed on 4 64-section systems: Aquilion-64, Brilliance-64, LightSpeed-64, and Sensation-64. All of the manufacturers

Table 1: Acquisition and reconstruction protocols and effective radiation dose for cochlear implant imaging on 64-section scanners

Variable	Aquilion 64	Brilliance 64	LightSpeed 64	Sensation 64
Acquisition protocol				
Tube voltage, kV	120	140	140	120
Tube current, mA	200	200	335	135
Beam collimation, mm	4×0.5	2×0.55	32×0.625	12×0.6
Pitch	0.75	0.5	0.531	0.45
Rotation time, s	0.5	0.5	0.6	1.0
Scan FOV	240	500	320	500
Dose of acquisition protocol				
Effective dose, mSv	1.4	2.0	1.8	1.3
Reconstruction protocol				
Section thickness, mm	0.5	0.55	0.6	0.6
Section interval, mm	0.3	0.3	0.3	0.3
Kernel	FC84	Filter D	BonePlus	U90u
Reconstruction matrix	512^2	768^2	512^2	512^2
Recon FOV PMMA phantom, mm		100		
Recon FOV PSF phantom, mm		50		
Recon FOV cadaver head, mm		80		

Note:—FOV indicates field of view; PMMA, polymethylmethacrylate; PSF, point spread function.

were asked to provide a specific, optimized protocol for inner ear CI imaging. The protocols were established by the manufacturer's own application specialist or by an experienced technician under the authority of the manufacturer and included both an acquisition and a reconstruction protocol. The specialists were present during the scans and able to vary the parameters to obtain an optimal protocol. These protocols were applied for the implanted human cadaver temporal bone, PSF, and PMMA phantom.

The main protocol parameters are listed in Table 1. Effective doses were calculated for all of the provided protocols with ImPACT CT patient dosimetry calculator (version 0.99x; available at www.impactscan.org) and are included in Table 1. All of the scans were repeated 3 times. Between the scans, both the object and the table were repositioned. A marker was fixed on each object to establish the same positioning in relation to the laser of the gantry in each scan and on each scanner.

The reconstruction fields of view (FOVs) were predefined for each object. A small image reconstruction interval was applied for the PSF phantom (0.1 mm on all of the systems) to accurately calculate the PSF.
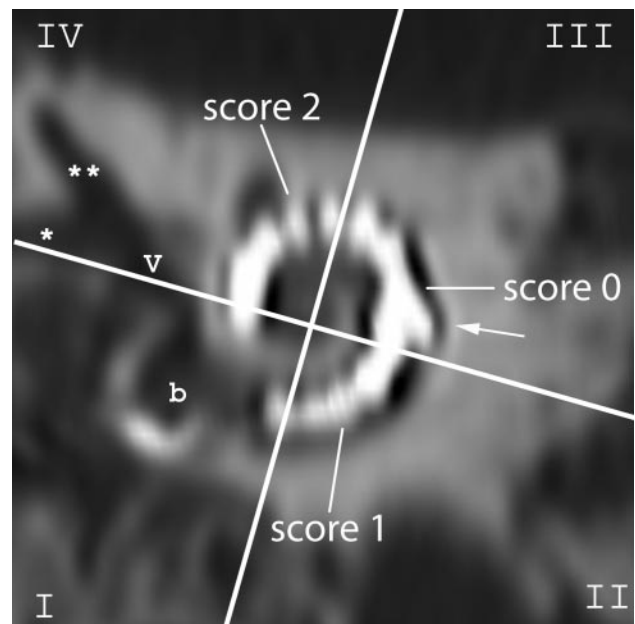
CI Electrode

A HiFocus1J electrode array, as is used in clinical practice, was implanted in the cadaver temporal bone and placed in the PMMA phantom. This electrode array consists of 16 electrode contacts, each measuring 0.4×0.5 mm with a contact spacing of 1.1 mm. The contacts are numbered from the tip of the electrode toward the base.
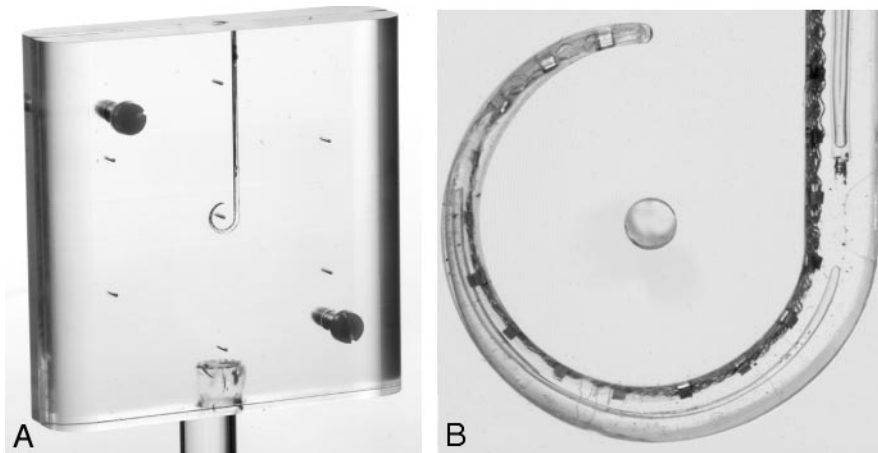
Ex Vivo Study

To mimic clinical conditions, a human cadaver temporal bone was scanned. It consisted of a $9 \times 9 \times 6$ cm^3 (anteroposterior, cranial-caudal, and right-left, respectively) segment of a human head, with the petrous bone in its center and including the auricle. The cadaver head was formalin fixed. The HiFocus1J electrode array was inserted by an experienced ear, nose, and throat (ENT) surgeon, following standard operating procedures. During insertion, an unusual resistance was felt. Contrary to clinical practice, the electrode was inserted further, resulting in a slight kinking of the array in the third quadrant of the cochlea (Fig 1).

To prevent postimplantation displacement, the electrode was

Fig 1. Scoring of the visibility of electrode contacts and anatomic structures: on a MPR perpendicular to the modiolus of an MSCT image of the implanted human cadaver temporal bone, the cochlea is divided in 4 quadrants (*white crosslines*). The quadrants are numbered counterclockwise, and the round window niche is located in the first quadrant (I-IV). A quantitative score from 0 to 2 was given to each electrode contact according to its visibility. Cochlear structures, such as the inner and outer wall, were scored per quadrant. The kinking of the electrode is localized in the third quadrant (*arrow*). b indicates basal turn of the cochlea at the level of the round window; v, vestibule, *horizontal semicircular canal (SCC); **superior SCC.

fixed by a single stitch and glue. To prevent CT artifacts from abrupt changes in attenuation, the cadaver temporal bone was placed in a $16 \times 16 \times 9$ cm^3 plastic container, submerged in gelatin (Merck, Darmstadt, Germany), and entrapped air was evacuated in a vacuum chamber. Gelatin was chosen to increase the attenuation of the human cadaver temporal bone to resemble the clinical setting. Axial CT images of the cadaver temporal bone were processed on a Vitrea work station (Vitrea 2; Vital Images, Minnetonka, Minn) according to the clinical protocol: multiplanar reconstructions (MPRs) perpendicular, as well as parallel, to the modiolar axis were made with contiguous
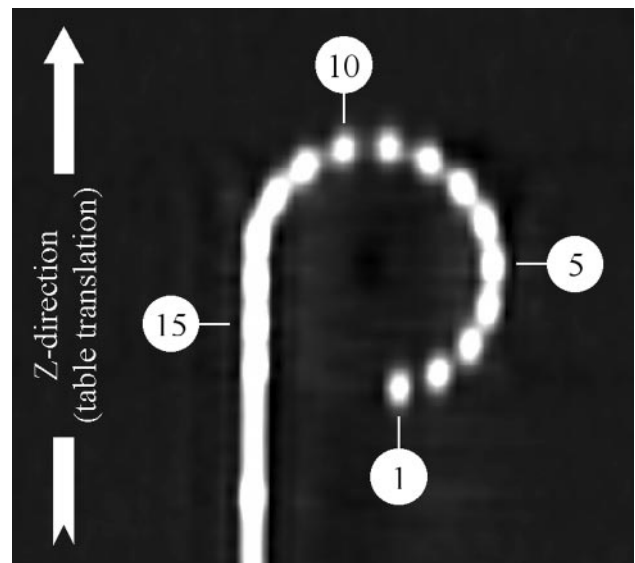
Fig 2. Photograph (*A*) and 1 high-resolution optical image (*B*) of the PMMA phantom containing a cochlear implant.

0.5-mm sections and subsequently stored. These MPRs were evaluated by 6 observers, 5 radiologists (a head and neck radiologist with 6 years of experience and 5 general radiologists with experience level 1–3 years), and 1 ENT surgeon with a 2-year experience in temporal bone imaging. They were blinded for the scanner brand. All of the images were presented in a random order. Window width and level could be adjusted by the observers. Postoperative imaging of CIs should provide information on the precise localization of the implant and its individual contacts, as well as the presence of complications. To examine whether the different scanners can provide this information, the visibility of the course and localization of the electrode array, the presence of a complication (kinking), and the visibility of the inner and outer wall of the basal turn of the cochlea per quadrant were assessed by using a visual analog scale (VAS) from 0 to 10. The distinction of individual electrode contacts was evaluated by using the following quantitative score. If an electrode contact could not be distinguished from the previous or following contact, a score of 0 was given. If the electrode contact was clearly separated from its neighboring contacts, a score of 2 was given. In case electrode contacts could be differentiated at the surface but not in the center, a score of 1 was given (Fig 1). For each observer, a cumulative score per scan was calculated by summation of the scores of the 16 contacts. Thus, for each electrode array, a score between 0 and 32 was calculated first on images perpendicular to the modiolar axis and, in addition, on images parallel to the modiolar axis. Mean values and SDs of all of the measurements were calculated. To investigate statistically significant differences, VAS results were analyzed by a paired 2-tailed Student *t* test. To reduce type I errors in multiple comparisons, a Bonferroni correction (for *n* = 6 comparisons) was applied. A *P* value of <.008 was considered significant for each comparison to maintain a global .05 significance level.

PMMA Phantom

To evaluate errors in localization of electrode contacts on CT images, a phantom study was performed. A PMMA phantom, containing a CI, was manufactured (Fig 2*A*). The well-described geometry of the phantom served as a reference for measurements in CT images. It consisted of 2 100- × 100-mm² slabs of 14-mm-thick PMMA. In 1 of the slabs, a groove was cut by using a 3D milling machine; the second slab served as a cover. The edges of the phantom were rounded to prevent streak artifacts in the reconstructed images. Because the diameter of the electrode carrier reduces from electrode 16 toward the tip, the size of the groove was adjusted along its path to assure a tight fit of the CI. Starting along a straight line, the trajectory was curved

Fig 3. MSCT of the PMMA phantom: 16 electrode contacts are numbered from the tip to the base: electrode numbers 1, 5, 10, and 15 are indicated.

from electrode 13 toward the tip such that the CI followed approximately a three-quarter turn. At the center point of this curve and 35 mm from center point, at the corners of a hexagon, holes were drilled as references markers. To identify the location of the center of the electrode surface within the phantom, a number of high-resolution optical images were acquired until optimal visualization of all of the electrode contacts was achieved (3367 dpi; Fig 2*B*).
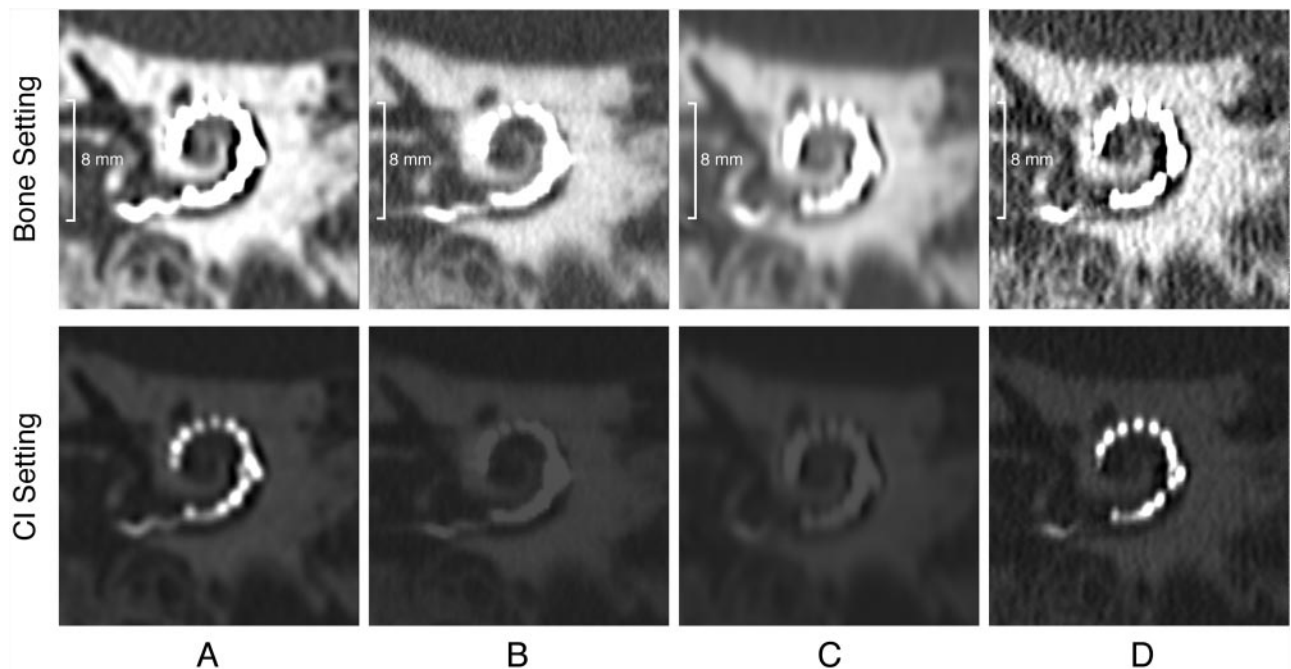
On these images, all 16 of the contacts were marked, and their positions were calculated relative to the phantom markers and groove wall. Based on these data, a computer model of the PMMA phantom was created for application in a MatLab based software (MatLab R2006a; MathWorks, Novi, Mich).

This in-house developed software calculated differences between electrode position as indicated by an observer and their known position in the phantom. For these measurements, MPRs were produced with the image plane parallel to the CI on a workstation (Anet64; Toshiba Medical Systems) by 4 observers (Fig 3, 1 head and neck radiologist with 6 years of experience and 3 physicists involved in CT). Two datasets were stored: one with a large FOV encompassing the 6 outer markers and another with a small reconstruction FOV containing the CI only. At first the computer model of the phantom, showing

Table 2: Results of the human temporal bone study

Scoring Parameters	Scoring Method	Aquilion 64	Brilliance 64	LightSpeed 64	Sensation 64
Overall impression	VAS	7.8 (1.0)	3.2 (1.0)	3.0 (1.1)	7.9 (0.7)
Axial oblique MPR, distinction of electrode contacts	Quantitative score	23.2 (2.7)	12.6 (4.4)	8.0 (3.9)	24.2 (4.8)
Coronal oblique MPR, distinction of electrode contacts	Quantitative score	23.7 (3.6)	14.2 (3.7)	10.2 (3.3)	25.6 (3.3)
Kinking	VAS	6.1 (2.1)	1.7 (1.5)	1.3 (1.2)	6.8 (2.0)
Inner cochlear wall 4 quadrants	VAS	6.9 (1.3)	4.9 (1.5)	4.1 (2.0)	6.2 (1.1)
		6.6 (1.1)	4.7 (1.3)	4.3 (1.7)	5.7 (1.4)
		6.2 (1.2)	3.9 (1.5)	3.9 (1.1)	5.3 (1.5)
		6.4 (1.4)	3.6 (1.7)	3.9 (1.4)	5.5 (1.9)
Outer cochlear walls 4 quadrants	VAS	7.7 (1.1)	6.8 (1.4)	5.5 (1.7)	7.4 (0.9)
		7.6 (1.2)	6.8 (1.1)	5.5 (1.5)	7.4 (1.0)
		7.1 (1.4)	5.2 (1.7)	4.6 (1.6)	6.8 (1.8)
		6.6 (1.9)	4.8 (1.8)	4.1 (1.8)	6.4 (1.9)

Note:—VAS indicates visual analogue scale; MPR, multiplanar reconstruction.

Fig 4. MPR CT images of the human cadaver temporal bone along the plane of the electrode array on Aquilion-64 (*A*), Brilliance 64 (*B*), LightSpeed-64 (*C*) (also seen in Fig 1), and Sensation-64 (*D*). The upper set of images is displayed with W/L 3000/800 and shows cochlear anatomic structures, such as the semicircular canals, well in all of the scanners. The lower set of images shows the chosen manually adjusted window/level setting for visualization of the electrode contacts. This illustrates that a wide range of HUs is essential for visualization of the CI.

only the position of the 7 markers, was fitted to the large FOV MPRs. Subsequently, by using the same center point, fitting parameters were applied to the small FOV MPR on which 4 observers marked the position of each electrode. The difference between electrode contact position as indicated by the observer and position in the computer model was calculated automatically. From these data, the absolute mean difference per electrode contact was calculated for each scanner.

PSF Phantom
For the PSF measurement, a phantom containing an iron bead with a diameter of 0.18 mm was scanned. Spatial resolution was quantified by measuring the full width at half maximum (FWHM) of the PSF curve. FWHM was measured in x- and y-directions (in-plane) and in z-direction (longitudinal).

All of the axial images were analyzed by an in-house developed MatLab-based script. From the axial images, binary images were calculated with a threshold at 1000 Hounsfield units (HUs). With the binary images, the center of the bead was determined followed by

recording of pixel values in 3 dimensions (x, y, and z) over a distance of 5 mm. To calculate the FWHM in relation to the background, a baseline correction on the resulting curves was performed. The FWHM was calculated for all of the curves. The mean FWHM for all of the repeated measurements per scanner was calculated in plane and in the longitudinal direction.

Results

Ex Vivo Study
Assessment results of the human cadaver temporal bone are summarized in Table 2. The average VAS score of the overall impression of the postoperative CT images was lower for Brilliance-64 and LightSpeed-64 relative to Aquilion-64 and Sensation-64 (Fig 4). A similar observation was made for the quantitative score of images perpendicular to the modiolar axis. Brilliance-64 and LightSpeed-64 images yielded limited information in the first projection. With the second projec-

Table 3: Results of PMMA phantom measurements				
Electrode Contact	Aquilion 64	Brilliance 64	LightSpeed 64	Sensation 64
1	0.07 (0.02)	0.11 (0.02)	0.07 (0.02)	0.03 (0.01)
2	0.05 (0.02)	0.12 (0.01)	0.09 (0.03)	0.05 (0.02)
3	0.09 (0.01)	0.13 (0.00)	0.09 (0.03)	0.06 (0.01)
4	0.10 (0.02)	0.09 (0.02)	0.14 (0.02)	0.08 (0.02)
5	0.12 (0.02)	0.07 (0.01)	0.10 (0.04)	0.09 (0.02)
6	0.11 (0.02)	0.09 (0.03)	0.12 (0.01)	0.09 (0.01)
7	0.11 (0.03)	0.09 (0.05)	0.13 (0.02)	0.10 (0.01)
8	0.14 (0.03)	0.07 (0.02)	0.20 (0.04)	0.13 (0.02)
9	0.13 (0.03)	0.08 (0.01)	0.18 (0.03)	0.13 (0.02)
10	0.14 (0.02)	0.10 (0.01)	0.16 (0.03)	0.12 (0.01)
11	0.08 (0.01)	0.10 (0.03)	0.12 (0.02)	0.08 (0.01)
12	0.11 (0.01)	0.13 (0.07)	0.15 (0.02)	0.10 (0.00)
13	0.10 (0.02)	0.15 (0.05)	0.25 (0.10)	0.09 (0.01)
14	0.10 (0.01)	0.10 (0.02)	0.24 (0.11)	0.11 (0.00)
15	0.11 (0.01)	0.12 (0.05)	0.31 (0.15)	0.10 (0.01)
16	0.11 (0.00)	0.16 (0.12)	0.61 (0.35)	0.12 (0.01)

Note:—PMMA indicates polymethylmethacrylate.

tion, some improvement in detection of individual contacts was obtained (2 points).

Kinking of the electrode was recognized in 68 of 72 scans. It was missed on Brilliance-64 images 3 times and once on a LightSpeed-64 scan by 2 different observers. When recognized, the VAS score of the exact course of the curled segment was highest in Aquilion-64 and Sensation-64 scans.

Assessment of the inner and outer walls of the basal turn of the cochlea showed a higher average VAS score for the outer wall in all of the quadrants and all of the scanners compared with the inner wall. Statistical analysis showed significantly lower VAS ($P < .008$) for Brilliance-64 and LightSpeed-64 compared with Aquilion-64 and Sensation-64.

PMMA Phantom
Differences between the positions of the electrode contacts as indicated by the observers compared with the position according to the computer model of the phantom are listed in Table 3 as mean values of their relative distance, calculated for 4 observers. Displacement of electrode contacts ranged from 0.05 to 0.14 mm (mean, 0.10 mm) on Aquilion-64, 0.07 to 0.16 mm (mean, 0.11 mm) on Brilliance-64, 0.07 to 0.61 mm (mean, 0.18 mm) on LightSpeed-64, and 0.03 to 0.13 mm (mean, 0.09 mm) on Sensation-64.

As graphically shown in Fig 5, the resulting differences in relative distance vary along the course of electrode array and differ between the 4 scanners (range, 0.03–0.6 mm). Increase in SD, which is more pronounced at basally located electrode contacts in Brilliance-64 and LightSpeed-64, indicates that observers were less consistent in localization. This is consistent with the fact that they reported to be less confident in these cases. Neglecting the most inaccurate measurements with the highest SD (most basal contacts, 12–16), the displacement of electrode contact position was within the range of 0.03–0.20 mm.

PSF Phantom
PSF measurements on all of the systems reproduced well; the mean difference between repeated measurements was 0.00 ± 0.01 mm. FWHM in the x- and y-directions were closely re-
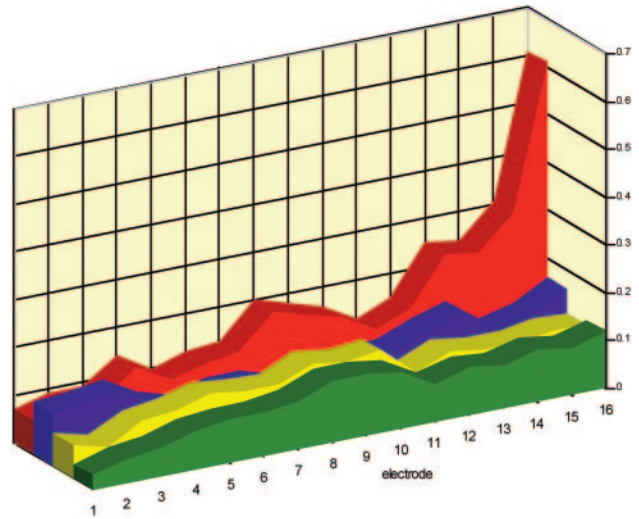

Fig 5. Graphic presentation of the mean differences over 4 observers (y-axis) between electrode position as manually indicated and the position in the computer model (in millimeters). Values are shown per electrode contact (x-axis) for each scanner (Aquilion-64, *yellow*; Brilliance-64, *blue*; LightSpeed-64, *red*; Sensation-64, *green*). See also Table 3.

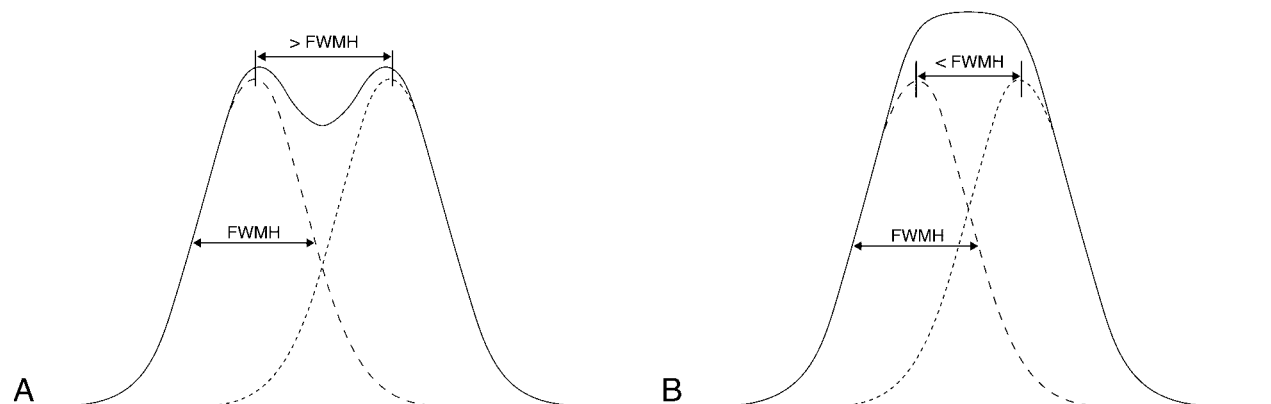| Table 4: Results of PSF measurements				
	FWHM, in mm			
Variable	Aquilion 64	Brilliance 64	LightSpeed 64	Sensation 64
In-plane	0.68	0.52	0.68	0.48
Longitudinal	0.81	0.84	0.98	0.70
Ratio in-plane/longitudinal	0.84	0.62	0.69	0.69

Note:—PSF indicates point spread function; FWHM, full width half maximum.

lated for all of the scans, with a mean difference of 0.00 ± 0.01 mm. The in-plane resolution was, therefore, calculated as the mean of x- and y-directions. On all of the scanners, in-plane FWHM was better than longitudinal FWHM (Table 4). The in-plane resolution varied from 0.48 to 0.68 mm and the longitudinal resolution from 0.70 to 0.98 mm over the 4 scanners.

Because of a limited available HU range, the maximum HU in the bead was reached on the Brilliance-64, impeding correct measurement of a small part of the top section of the PSF curve. The FWHM values were still calculated as accurately as possible. The maximum amount of improper pixel values was 5; the resulting PSF curve was cut off at the maximum available HU along a distance of 0.4 mm. It was estimated that the HU scale limitation on the Brilliance-64 may have resulted in an overestimation of FWHM values ≤0.05 mm.

Discussion
The demands for postoperative imaging in CI surgery became higher over the last years. At first, imaging was used for confirmation of intracochlear position without kinking and integrity of the electrode array. To obtain a better understanding of the postoperative speech perception results and to assess new developments in electrode designs and differences in surgical techniques, a more detailed analysis of the postoperative status was needed. Both the exact position of individual electrode contacts, as well as the morphology of the cochlea, should be visualized. This study was undertaken to evaluate whether it is possible to obtain qualitatively acceptable images of implanted cochleas with 64-section CT scanners of 4 major vendors. Pos-

Fig 6. Clinical implications of the PSF: the *dotted curves* depict the pixel value of a single electrode contact through the center. Summation of these curves renders a curve (*black line*). When the distance between 2 electrodes is larger than FWHM, the resulting curve still shows 2 maximum values, and the electrode contacts can be separated in the image (*A*). If the distance between 2 electrode contacts is smaller than FWHM, the resulting curve shows a single peak; the electrode contact cannot be visualized separately (*B*).

sible limitations are the inherent scanner resolution, image distortion because of metallic artifacts, the scanner-dependent reconstruction algorithm, and the lack of a sufficient wide range of available HUs for displaying structures of high attenuation.

PSF phantom measurements were performed to evaluate whether the inherent resolution of the scanners is high enough to visualize individual electrode contacts. The outcome of the measurements of the in-plane and longitudinal resolution indicates that current CT scanners offer just enough spatial resolution to visualize individual electrode contacts in the images of the CI evaluated in this study. Because the diameter of the electrode contacts in the investigated CI electrode is somewhat smaller than the measured FWHM of the PSF, we can consider the individual contacts approximately as point sources. In this case, the FWHM indicates the minimum intercontact distance at which the contacts can be distinguished separately in the resulting images. As illustrated in Fig 6, an intercontact distance lower than the FWHM results in an intensity distribution that inhibits visualization of individual electrode contacts. Given a longitudinal resolution that ranges from 0.70 to 0.98 mm, it should be possible to visualize the individual electrodes of the HiFocus1J electrode array, which has an electrode spacing of 1.1 mm. However, the CI is curved when following the trajectory of the cochlea, and, as a result, the actual distance between electrodes may become less than the spacing that is measured along the curvature. Separate visualization of electrode contacts may become critical or may even be beyond reach in some scanners, especially closer to the apex, when curvature becomes stronger. For implants with tighter electrode spacing, such as the Contour Advance (Cochlear, Sydney, Australia), with intercontact distance that decreases from base to apex from 0.72 to 0.40 mm, visualization of separate electrodes will present a challenge at the most apical contacts.

Image degradation because of metallic artifacts, measured as displacement of the center of an electrode contact in the PMMA phantom, was dependent on the localization of the contact within the electrode array. The artifacts can be ascribed to scanner resolution and scanner-dependent reconstruction kernel. As shown in the PSF phantom measurements, the z resolution is somewhat lower than the in-plane

resolution. This can contribute to deterioration in the separation of individual electrode contacts along the electrode array in the longitudinal direction. In clinical scanning, the precise localization of contacts will differ, depending on the orientation of the CI trajectory relative to the z-direction.

The measurement of the electrode contact position was less consistent and showed higher SD at the most basal contacts 12–16 in Brilliance-64 and LightSpeed-64. This decrease in accuracy is possibly explained by the structural changes of a CI along its length. Whereas in the apex only contacts connected by a fine wire are seen, in the base, several wires, including these connected to apical contacts, are bundled alongside the electrode contacts. The higher amount of metallic material might cause additional distortions. As stated above, this mostly affects the scanners with a lower z resolution. It is as yet unclear which maximal error in the localization of contacts is clinically acceptable.

Independent of the trajectory of the CI electrode, the visibility of the outer wall of the cochlea was rated better than the visibility of the inner wall or modiolus. This is most probably based on the underlying anatomic substrate. The outer wall is part of the otic capsule, consisting of attenuated bone only. The modiolus or central bony axis of the osseous cochlea contains some neural tissue and shows a distinctly lower attenuation. Therefore, contrast with the perilymph and endolymph in the cochlear lumen will be more distinct for the outer wall than for the inner wall.

Despite the scanty differences in resolution and distortion, the assessment of the human cadaver scans showed a very wide range among the 4 scanners. Both the subjective and quantitative scores showed a clear preference for 2 scanners (Aquilion-64 and Sensation-64). This counts for the overall appreciation of the images, as well as for the visualization of individual electrode contacts and cochlear walls. Other than the above-mentioned differences in resolution, one of the contributing factors to diversity in image appreciation is the use of different reconstruction kernel types. Various reconstruction kernel types were applied by the manufacturer's specialists, and the following were chosen to be the most appropriate: soft kernel (LightSpeed-64), intermediate kernel (Aquilion-64 and Brilliance-64), and sharp kernel (Sensation-64). Another limiting factor is the available range of HUs. Because the densities of

the evaluated structures differ considerably, a large window width and window level are needed to accurately visualize the electrode contacts (typically 16,000/6000). The available range of HUs is −32,768 to 32,767 for Aquilion-64, −1024 to 2976 for Brilliance-64, −1024 to 3070 for Lightspeed-64, and −10,240 to 30,710 (extended HU scale) for Sensation-64. Scanners with a restriction in available HU range (Brilliance-64 and LightSpeed-64) received lower scores despite having a FWHM value that is lower than the maximum intercontact distance. Thus, a major cause of the lower appreciation seems to reside in the limited range of available HUs, resulting in an abrupt cutoff of the associated gray values in the images.

The limited HU display capabilities led 4 times to missed kinking. Kinking is a possible complication in implant surgery that influences the stimulation selectivity and can require program changes in the speech processor. Considering the technical abilities of these scanner systems, it seems very plausible that an adjustment of the software, that is, extension of the Hounsfield range, will reduce the described problems in postoperative imaging of CIs.

Of all of the above-mentioned factors related to the performance of the scanners, the wide range of HUs in the images plays the most important role in the overall appreciation of the individual electrode contacts in postoperative imaging of the HiFocus1J electrode array. Thus, the limiting factor is mainly a matter of software improvement and is not related to the fundamental mechanical features of the different scanners.

Conclusions

Imaging protocols for postoperative imaging after cochlear implantation as advised by application specialists or technicians under supervision of the manufacturers of 4 different 64 section CT scanners are presented. Based on the PSF results, HiFocus1J electrode contacts can be visualized separately on all of the studied scanners. However, when the curvature of the implant causes narrowing of the intercontact spacing to <1 mm, separate visualization of electrode contacts might become critical on LightSpeed-64 (longitudinal resolution for LightSpeed-64, 0.98 mm). Assessment of CI visibility, as well as the quantitative assessment of electrode contact positions, varies between scanners. It seems plausible that software adjustments allowing for a wider range of HUs will be needed in 2 scanners to improve image quality for a possible higher diagnostic value.

References

1. Verbist BM, Frijns JHM, Geleijns J, et al. **Multisection CT as a valuable tool in the postoperative assessment of cochlear implant patients.** *AJNR Am J Neuroradiol* 2005;26:424−29
2. Aschendorff A, Kubalek R, Hochmuth A, et al. **Imaging procedures in cochlear implant patients– evaluation of different radiological techniques.** *Acta Otolaryngol* 2004;suppl:46−49
3. Tange RA, Grolman W, Maat A. **Intracochlear misdirected implantation of a cochlear implant.** *Acta Otolaryngol* 2006;126:650−52
4. Jain R, Mukherji SK. **Cochlear implant failure: imaging evaluation of the electrode course.** *Clin Radiol* 2003;58:288−293
5. Mecca MA, Wagle W, Lupinetti A, et al. **Complication of cochlear implantation surgery.** *AJNR Am J Neuroradiol* 2003;24:2089−91
6. Skinner MW, Ketten DR, Holden LK, et al. **CT-derived estimation of cochlear morphology and electrode array position in relation to word recognition in nucleus-22 recipients.** *Jaro* 2002;3:332−50
7. van der Beek FB, Boermans PP, Verbist BM, et al. **Clinical evaluation of the Clarion CII HiFocus 1 with and without positioner.** *Ear Hear* 2005;26:577−92
8. Cesarini F, Gallizioli M, Solero P, et al. **Double array cochlear implant: CT findings.** *Radiol Med (Torino)* 2002;103:115−18
9. Xu J, Xu SA, Cohen LT, et al. **Cochlear view: postoperative radiography for cochlear implantation.** *Am J Otol* 2000;21:49−56
10. Whiting BR, Bae KT, Skinner MW. **Cochlear implants: three-dimensional localization by means of coregistration of CT and conventional radiographs.** *Radiology* 2001;221:543−49
11. Chen JM, Farb R, Hanusaik L, et al. **Depth and quality of electrode insertion— a radiologic and pitch scaling assessment of two cochlear implant systems.** *Am J Otol* 1999;20:192−97
12. Husstedt HW, Aschendorff A, Richter B, et al. **Nondestructive three-dimensional analysis of electrode to modiolus proximity.** *Otol Neurotol* 2002;23: 49−52